Journal of The Electrochemical Society, **152** (11) H183-H190 (2005)
0013-4651/2005/152(11)/H183/8/$7.00 © The Electrochemical Society, Inc.

Investigation of Fluorescence Degradation Mechanism of Hydrated $BaMgAl_{10}O_{17}:Eu^{2+}$ Phosphor

K. C. Mishra,[a,*,z] M. Raukas,[a,*] G. Marking,[b] P. Chen,[c] and P. Boolchand[c]

[a]*Osram Sylvania, Central Research, Beverly, Massachusetts 01863, USA*
[b]*Osram Sylvania, Precision Materials and Components, Towanda, Pennsylvania 18848, USA*
[c]*Department of Electrical Engineering, Computer Engineering and Computer Science, University of Cincinnati, Cincinnati, Ohio, USA*

We have investigated the degradation of $BaMgAl_{10}O_{17}:Eu^{2+}$ phosphor (BAM) using ^{151}Eu Mössbauer and fluorescence spectroscopic methods. The ^{151}Eu Mössbauer measurements show that upon hydration, a significant fraction of divalent europium ions is oxidized. The degradation process induced by the intercalated water molecules into the host lattice appears to be a unique process. It has many features that are both similar to and distinct from those induced by oxidation in air and those caused by discharge during the lamp life. A plausible mechanism of degradation of BAM caused by the intercalated water molecules is discussed.
 [DOI: 10.1149/1.2041927]

Manuscript submitted March 31, 2005; revised manuscript received May 12, 2005. Available electronically September 14, 2005.

The barium magnesium aluminate phosphor activated by divalent europium ions (BAM) continues to be a subject of great interest in the fluorescence community because of its importance as an efficient blue-emitting phosphor. However, its relative instability in a variety of lamp-related processing conditions and also during the lamp life continues to be a major concern.[1-7] A better alternative to this blue-emitting phosphor has yet to be developed. Therefore, a great deal of attention is focused worldwide on understanding the underlying mechanisms of various degradation processes. It is hoped that such an understanding could help in improving the maintenance of this phosphor. The present paper reports results from a study involving degradation of BAM induced by intercalated water molecules.

Intercalation of water into the host lattice of BAM ($BaMgAl_{10}O_{17}$) has been reported to play a critical role in the degradation process of this blue-emitting phosphor.[6,7] The baking steps during the fabrication of fluorescent lamps and plasma display panels produce conditions favorable for intercalating water molecules into the β-alumina lattice of BAM. Intercalation of water molecules at the baking temperature (~400–500°C) has been observed, causing oxidation of Eu^{2+} ions and color shift of the phosphor emission.[6] It has also been proposed that the water molecules contribute to degradation of the phosphor during the lamp life.[6]

The degradation process induced by water molecules during lamp baking has many features that are both similar to and distinct from those resulting from the oxidative degradation of BAM from firing in air or degradation during the lamp life. One observes a blue shift of the main emission peak from BAM near 450 nm caused by oxidation of the activator ions by firing in the air. In contrast, the emission spectrum of hydrated BAM shifts toward the green region of the visible spectrum after baking accompanied by a long tail extending to the deep red. This color shift is usually observed during aging of this phosphor in mercury discharge lamps.

Poor maintenance and loss of brightness of hydrated BAM are attributed mainly to oxidation of europium ions during the baking process[6] in addition to absorption of ultraviolet (UV) radiation from discharge by the water molecules and vibronic coupling of divalent europium ions with adjacent water molecules.

It has been observed that water molecules can be easily intercalated into the intermediate plane of aluminates in the β-alumina structure.[8] Using X-ray and neutron diffraction methods and infrared spectroscopy, Bates et al. investigated the location and geometry of water molecules in lithium β-aluminate.[8,9] The relative openness of the intermediate plane in the β-alumina lattice is considered to be responsible for the observed absorption of water. The diffraction measurements locate the water molecules in this plane.[8] That the water molecules are inside the bulk material is also confirmed by the observation of the infrared stretching frequency near 2881.2 cm^{-1} which is distinct from the corresponding vibrational frequencies of water molecules adsorbed on the surface.[6] Additionally, a significant fraction of the adsorbed water molecules is also believed to be dissociating to OH^- and $[(H_2O)_xH^+]$ groups. These molecular groups are located within the β-alumina lattice.[6,8]

A proper understanding of the degradation process induced by the intercalated water molecules begs a complete picture of the structure, location, and geometry of water molecules in the BAM lattice, direct evidence of the generation of trivalent ions, and a thorough characterization of the fluorescence spectra of fresh and degraded phosphor samples. With the availability of this information, a coherent picture of the degradation process can be developed, and the underlying chemical processes can be explored to prevent the degradation process. In a related theoretical study,[10] the structural questions regarding the intercalated water molecules were studied using atomistic simulation methods and possible mechanisms of the oxidation processes were explored. In the present paper, we have probed the fresh and hydrated samples by ^{151}Eu Mössbauer spectroscopy and solid-state fluorescence techniques to establish the growth of trivalent europium ions during the hydration process and spectroscopic characterization of the degradation process.

Sample Preparation

The BAM phosphor used in this work was obtained from the BAM phosphor lot (SSX-1) prepared for plasma display panel (PDP) application, and is referred to as PDP BAM. The formulation is almost stoichiometric. The material has a blue emission color. The starting mixture was composed of 10.5 mol % $Al(OH)_3$, 1.05 mol % $MgCO_3$, 0.83 mol % $BaCO_3$, 0.09 mol % BaF_2, and 0.04 mol % Eu_2O_3. In order to produce material with the small particle size necessary for use in PDPs, we use small particle size Hydral 710 aluminum hydroxide. The $MgCO_3$ weight is corrected for a 97% assay; all other materials had an assumed assay of 100%. The materials are weighed into a drum and drum blended for 30 min. The material was fired in a standard square Pell tray on a C. I. Hayes type MY-6013130 continuous furnace at 1650°C under reducing conditions. The phosphor was wet-milled in 3.5 kg batches for 55 min on a small Sweco M-18 mill using low-density alumina media and then wet-sifted by 378 mesh. The material was then filtered, dried, and sifted through 64 mesh to break up the dried cakes. The particle size distribution exhibits a 50% size of 2.74 μm with 99.93% $<$ 9 μm.

The humidity treatment was performed as follows. Approximately 11.2 g of phosphor were placed in two small silica boats (~0.5 × 0.5 × 4.0 in.), which were loaded into a 3-in. diam quartz tube inside a tube furnace. The ends of the tube were partially sealed

* Electrochemical Soceity Active Member.
z E-mail: kailash.mishra@sylvania.com

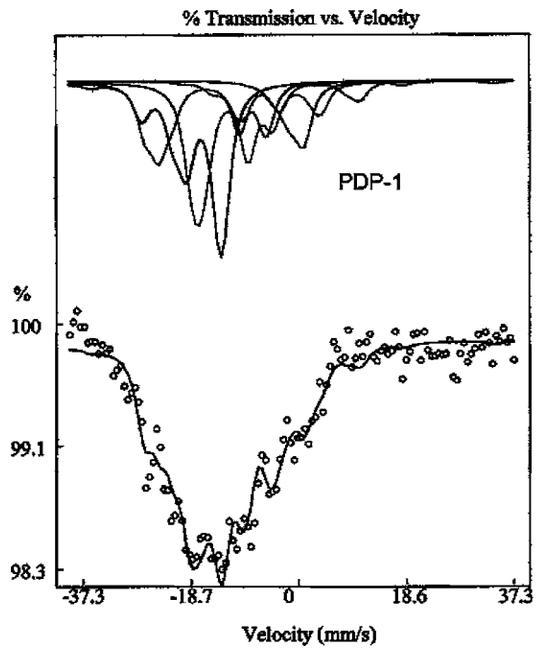

Figure 1. ^{151}Eu Mössbauer spectrum of a fresh PDP BAM phosphor sample.

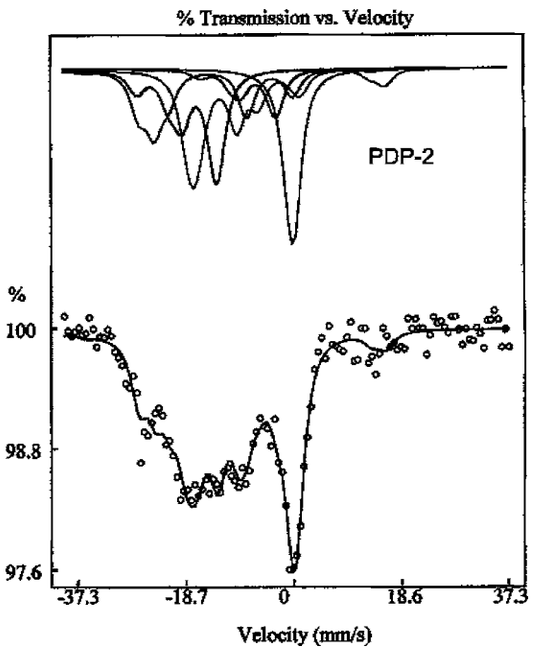

Figure 2. ^{151}Eu Mössbauer spectrum of a PDP BAM phosphor sample after hydration. Note the sharp peak near 0 mm/s corresponding to the trivalent europium ions.

concurrent with the ends of the hot zone by using shaped pieces of porous furnace brick. Humid air was prepared by bubbling compressed air through warm water (approximately 60°C). It was then introduced into the sample chamber using a small glass tube inserted through an opening in one of the furnace brick pieces. The furnace temperature was rapidly raised to 425°C and that temperature maintained for 2 h. At the end of this time period, the gas flow was terminated. The sample chamber was removed from the furnace and was allowed to cool under ambient conditions.

The vacuum ultraviolet (VUV) degradation of the hydrated BAM phosphor was performed for 1 h in a Xe-discharge environment, VURAAC. The VURAAC is a 100-cm loop of 5 cm inside diameter (i.d.) Pyrex tube that contains about 5 mT of flowing Xe and receives about 270 W of input power (~8.75 A and 31 V) at 450 kHz. A fixed flow rate and uniform pressure in the chamber are assured by choked flow through a needle valve inlet and an almost-closed gate valve outlet. The discharge is inductively coupled to minimize contamination from sputtering of the walls or electrodes. Approximately 90 mW/cm^2 of 147 nm VUV of about 6.7×10^{16} photons/(cm^2 s) is estimated to be incident on the sample surface. No significant excimer emission is generated under these operating conditions.

Phosphor samples were introduced as plaques using sample holders made of Macor machineable ceramic (a synthetic mica/borosilicate glass composite). These were carried on a $22 \times 1\frac{1}{4}$ in. strip of 6-mm Pyrex glass.

^{151}Eu Mössbauer Measurements

^{151}Eu Mössbauer spectroscopy measurements with the 21.64 keV gamma rays made use of ^{151}Sm with a half-life of 87 years in SmF_3 matrix (emitter) and a thin NaI scintillation counter. The Eu-doped phosphor (absorber) and the emitter were cooled to 4.2 K in an exchange gas liquid helium dewar. Standard transmission measurements were performed using a constant acceleration drive.

In general, the spectra revealed significant hyperfine structure (Fig. 1 and 2) similar to those of BAM samples reported earlier.[5] The observed line shapes were analyzed in terms of a superposition of multiple sites, with each site being represented by a 12-line pure quadrupolar pattern characteristic of the $7/2^+ \rightarrow 5/2^+$ spin sequence. The justification for multiple sites for europium ions in BAM has been discussed extensively in earlier publications. The quadrupolar pattern was parameterized in terms of the nuclear quadrupole coupling, e^2QVzz, isomer shift (δ), asymmetry parameter of the electric field gradient (η), and linewidth (Γ). In general, to deconvolute the observed line shape a minimum of five or more sites were found necessary for the results obtained at 4.2 K.

Figures 1 and 2 show the ^{151}Eu Mössbauer spectral line shapes for BAM phosphor samples before and after hydration, respectively. The well-defined peak near 0 mm/s in Fig. 2 reflects increasing Eu^{3+} ion concentration due to intercalation of water. Tables I and II provide a summary of fitting parameters for the ^{151}Eu Mössbauer

Table I. ^{151}Eu Mössbauer parameters for PDP BAM at 4.2 K (8% Eu) Γ = 2.9421 ± 0.0046 mm/s, χ^2 = 1.08.

Site	IS (mm/s)	e^2qQ (MHz)	η	% Distribution
1	−17.33 ± 0.13	840.50 ± 24.95	0.25	30
2	−11.23 ± 0.15	−1311.22 ± 29.66	0.01	30
3	−14.40 ± 0.02	−2153.64 ± 47.86	0.05	21
4	−8.23 ± 0.44	552.23 ± 81.49	0.4	9
5	−0.54 ± 0.47	340.65 ± 82.04	0.01	10

Table II. ^{151}Eu Mössbauer parameters for hydrated PDP BAM at 4.2 K (8% Eu) Γ = 2.9421 ± 0.0046 mm/s, χ^2 = 0.90.

Site	IS (mm/s)	e^2qQ (MHz)	η	% Distribution
1	−17.14 ± 0.18	846.25 ± 35.14	0.25	22
2	−11.86 ± 0.17	−1141.178 ± 32.36	0.01	26
3	−12.81 ± 0.21	−2464.91 ± 44.72	0.05	23
4	−6.81 ± 0.42	788.94 ± 85.27	0.4	10
5	−0.07 ± 0.11	79.53 ± 38.55	0.01	19

Table III. ^{151}Eu Mössbauer parameters for OSI BAM at 4.2 K (12% Eu) (40 min of oxidation in air) Γ = 3.50 ± 0.01 mm/s, χ^2 = 1.6102.

Site	IS (mm/s)	e^2qQ (MHz)	η	% Distribution
1	−17.73 ± 0.10	822.85 ± 12.78	0.25	25
2	−12.28 ± 0.10	−1068.06 ± 16.10	0.01	22
3	−13.52 ± 0.11	−2533.08 ± 20.61	0.05	21
4	−7.99 ± 0.15	863.72 ± 27.95	0.4	11
5	−0.48 ± 0.32	−1472.56 ± 63.20	0.01	5
6	0.65 ± 0.07	178.26 ± 16.67	0.01	16

line shapes for the two phosphor samples. As mentioned earlier, the fitting procedure used isomer shift (IS), nuclear quadrupole coupling constant (e^2qQ), asymmetry parameter (η), and the linewidth (Γ) as free parameters. The linewidth was assumed to be the same for each site. The distribution of europium ions among various sites has been calculated by assuming that europium ions occupying each site have the same recoil-free fraction at 4.2 K. Using χ^2 analysis, we observed that a pentamodal distribution of sites with nuclear quadrupolar broadening provides the best fit for the observed line shape. Each site contributes twelve Lorentzians with identical linewidths and appropriate branching ratios.

ISs provide a good measure of the oxidation state of the europium ions. The observed five sites can be classified into three distinct types: sites with divalent europium ions with IS ranging approximately from −18 to −11 mm/s, a site with IS close to 0.0 mm characteristic of trivalent europium ions, and a site with IS near 8.0 mm/s, intermediate to divalent and trivalent Eu. On the basis of the observed nuclear quadrupole coupling constants and calculated field gradients by first-principles methods, the three divalent europium sites have been identified as mid-oxygen (mO), Beevers-Ross (BR), and anti-Beevers-Ross (a-BR) locations in the intermediate plane of the β-alumina structure.[11] These locations correspond to sites 1, 2, and 3 in Tables I-V, respectively. The percentage occupancy of these sites along with those for the other two sites in the PDP BAM sample before hydration is comparable to those reported for BAM with 12% Eu. The locations of the two other sites are not precisely known. The oxidation state of the Eu ions at the site with IS close to −8 mm/s is also not known. It could be either a metallic state or a mixed valence state. It is speculated to be the latter in Ref. 5.

In the case of untreated BAM, 81% of the europium ions are located at the divalent sites with 10% being at the trivalent sites. When the phosphor is hydrated, the divalent ion occupancy decreases by 10%, accompanied by 9% increase in the occupancy of trivalent site. This is almost twice the amount in the trivalent ions for regular BAM after 40 min of oxidation in air at 600°C. The occupancies of sites 1 and 2 decreased after intercalation of water, while that of site 3 remained unaffected or increased slightly from 21 to 23%, indicating stability of this type against oxidative degradation compared to other two sites.

Table IV. ^{151}Eu Mössbauer parameters for OSI BAM at 4.2 K (12% Eu) (after 1400 h in lamp- the sample is the same as Table V) Γ = 3.07 ± 0.0049 mm/s, χ^2 = 1.20.

Site	IS (mm/s)	e^2qQ (MHz)	η	% Distribution
1	−17.13 ± 0.12	875.35 ± 22.49	0.25	28
2	−11.91 ± 0.13	−993.94 ± 24.97	0.01	27
3	−13.13 ± 0.18	−2347.72 ± 38.23	0.05	21
4	−7.41 ± 0.28	565.43 ± 53.34	0.4	12
5	0.51 ± 0.22	−246.13 ± 47.03	0.01	12

Table V. ^{151}Eu Mössbauer parameters for OSI BAM at 4.2 K (12% Eu) (after 0 h in lamp) Γ = 2.88 ± 0.0046 mm/s, χ^2 = 1.0576.

Site	IS (mm/s)	e^2qQ (MHz)	η	% Distribution
1	−17.78 ± 0.15	857.75 ± 28.65	0.25	23
2	−11.99 ± 0.12	−1142.80 ± 23.88	0.01	30
3	−13.47 ± 0.16	−2531.06 ± 35.20	0.05	24
4	−6.68 ± 0.28	1119.84 ± 58.82	0.4	13
5	0.39 ± 0.39	−1030.71 ± 75.60	0.01	10

In addition to increasing concentration of trivalent europium ions following intercalation of water, both IS and nuclear quadrupole coupling constant significantly changed for sites 2 and 3. These parameters do not change appreciably for site 1. The change in IS for site 3 indicates a net transfer of charge from the divalent europium ion to its neighboring ions. For both sites 2 and 3, the nuclear quadrupole coupling constants change significantly, implying changes in the electronic structure of the divalent ions located at these sites either due to a rearrangement of neighboring ions or addition or removal of ions from the neighborhood. Because we do not treat the asymmetry parameters as free parameters for hydrated samples and used the same values from virgin samples, it is not possible to comment on how intercalated water molecules or hydroxy groups could have affected the local symmetry.

It is worthwhile to examine how changes in the electronic structures of europium ions caused by intercalation of water molecules differ from those due to oxidation of europium in air or aging inside the lamps. These studies were performed using BAM phosphor samples with 12% europium. The fitting parameters for both the cases are shown in Tables III and IV. Because the fitting parameters for virgin BAM samples are similar to those in Table I, they are not included for comparison.

The results for oxidized samples correspond to those of a BAM phosphor sample after 40 min of oxidation at 600°C. The changes in IS and e^2qQ for the divalent europium ions is almost similar to that for hydrated BAM. The most noticeable difference is with respect to trivalent ions. The isomer shift of site 6, which develops with firing in air, is more positive than that for the trivalent ions for the hydrated BAM. It is also interesting to note an earlier observation that BAM samples always contain some trivalent europium ions. In fresh samples, the trivalent europium ions are characterized by an IS that is usually negative, while those for the oxidized samples are slightly positive. In the case of oxidation in air, the trivalent ions are readily converted to sites with slightly positive IS. Only in one fresh sample, we observed the simultaneous presence of two different types of trivalent europium ions within the tolerance limit of data fitting procedure.[15] In the case of hydrated BAM, the IS of the Eu^{3+} site showed a similar shift with respect to the fresh BAM sample.

In Table IV, we have listed the Mössbauer effect results for a phosphor sample exposed to discharge for 1400 h in lamps with higher ultraviolet flux. This phosphor sample is a good representation of an aged sample whose degradation is caused by both baking and exposure to UV radiation and ion bombardment. Undoped samples show development of color centers for similar exposure to lamp environment. In Table V, we have also shown the Mössbauer effect parameters for a phosphor sample with identical composition after 0 h, oxidative heating steps of a fluorescent lamps. It is important to note that the concentration of trivalent ions has not changed significantly in the aged sample even after an exposure of 1400 h to the discharge. Thus, the degradation in aged samples is definitively not due to oxidation of europium ions. The ISs for the trivalent ions have a positive shift with respect to a 0 h sample, similar to the case found in the case of hydrated BAM. These observations suggest that hydration of BAM probably affects the phosphor at 0 h. The degradation in aged lamps is most likely a different mechanism. It is possible that intercalation of water leads to a degradation of the

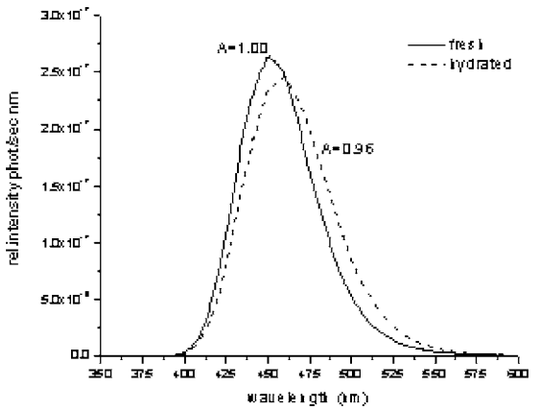

Figure 3. Emission spectra of as-received (solid line) and hydrated PDP BAM (dashed line) for 250-nm excitation. About 4% relative change in total integrated area has been indicated.

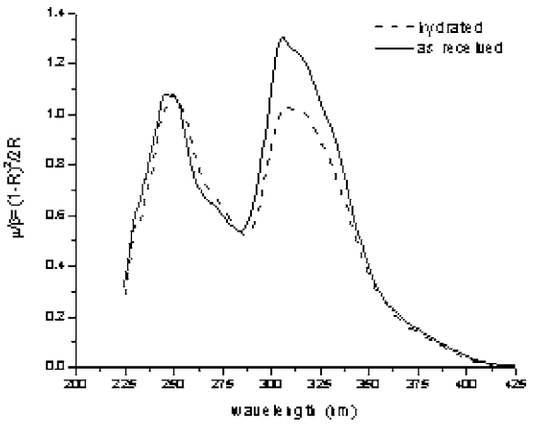

Figure 4. Spectra of absorption (remission function) $\mu/\beta = (1 - R_\infty)^2/2R_\infty$ of as-received and hydrated PDP BAM in thick plaques. Note the regions where absorption has increased (255–285 nm) and reduced (290–350 nm) upon treatment with water vapor.

phosphor composed of two effects: oxidation of BAM and modification of electronic structure of divalent europium ions due to water molecules or hydroxyl groups in the vicinity.

Fluorescence Measurements

We measured fresh, hydrated, and VUV-irradiated PDP BAM samples in SPEX Fluorolog-2 spectrometer at room temperature for reflectance, emission, and excitation spectra. All materials were compared against plaques of Al_2O_3 powder (Alfa Aesar) which were in turn measured with respect to a standard obtained from LabSphere. The emission spectra were also acquired under 147-nm excitation from a Xe discharge in VURAAC. Liquid helium temperatures, when needed, were achieved by CTI closed cycle cryostat. All the spectra are corrected for the measurement system response.

The typical emission band of BAM peaking at around 450 nm is due to $4f^65d$-to-$4f^7$ transitions of Eu^{2+}. For 250-nm excitation, the emission spectrum is broadened and the peak shifted after the water treatment, as shown in Fig. 3. The peak is located now at 460 nm, and the full width at half maximum (fwhm) of the emission band increased from approximately 50 to 60 nm (2520–2850 cm^{-1}). The total integrated emission intensity (in photons s^{-1}) of the infinitely thick plaques for this excitation remained the same within a few percent compared to the untreated sample. Additional VUV irradiation in VURAAC did not add any remarkable spectral changes under 250-nm excitation, except for slightly higher intensity in the long wavelength tail. A careful examination of the hydrated sample upon cooling to 15 K revealed only weak red emission characteristic of Eu^{3+} upon 250-nm excitation. We think that the luminescence of Eu^{3+} in $BaMgAl_{10}O_{17}$ is generally not observable, although its presence is verified in oxidized and hydrated samples by ^{151}Eu Mössbauer spectroscopy.

Reflectance exhibited almost no changes upon hydration at 250 nm. In Fig. 4 we present the remission function $m(\lambda)$ that is proportional to the absorption coefficient of the material μ and is calculated based on the Kubelka-Munk theory as $m = \mu/\beta = (1 - R_\infty)^2/2R_\infty$, where R_∞ is the reflectance of thick plaques and β the scattering coefficient. In the range of 255–285 nm, one notices an increase in m, suggesting the appearance of new absorption band(s). In contrast, there is a drop in remission at 290–350 nm that can be attributed to disappearing Eu^{2+} absorption at these wavelengths. The consequences of these observations are discussed later. Excitation spectra (for monitoring the emission at 450 nm from thick plaques, Fig. 5) present the same overall shape for the as-received, hydrated, and VUV-irradiated samples. On normalizing at 305 nm, one observes reduced efficiency for hydrated and irradiated samples for $\lambda < 295$ nm and from 330 to 410 nm. As discussed in detail earlier,[4,12] highly doped BAM exhibits a number of excitation bands that are strongly broadened and overlapping. One could estimate the locations of main features at 250, 275, 305, 330, and 375 nm. As an exception, the VURAAC-irradiated BAM powder that has previously been hydrated shows a new excitation feature appearing at approximately 205 nm. This excitation band is absent in other samples.

Using ethanol suspensions, we also prepared thin coatings of phosphor samples for fluorescent measurements. A comparison of fresh and water-treated materials in this case shows a decrease in emission and an increase of approximately 5–15% in reflectance due to hydration. This change in reflectance depends on the spectral region, coating thickness, and uncertainties in preparation method. Changes in excitation are qualitatively similar to the ones measured for thick plaques. For thin coatings of even as-received phosphor, the excitation band at 250 nm is weaker relative to the 305 nm one. This could be explained qualitatively assuming that it takes a considerably longer path length (larger thickness) in PDP BAM powder for a 250-nm photon to get absorbed and generate the same amount of blue photons than for the photon at 305 nm.

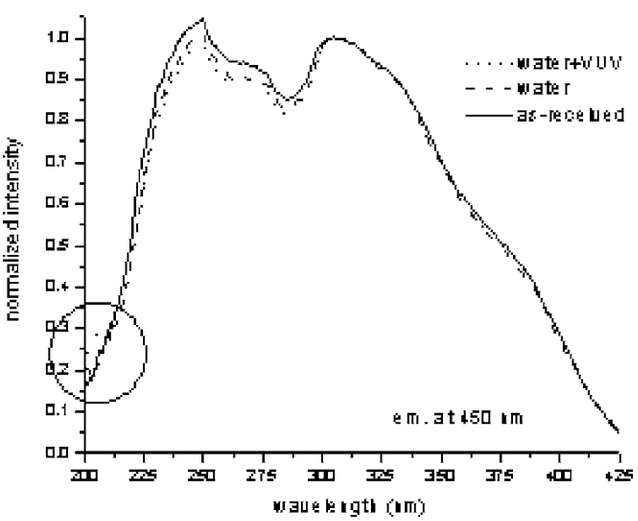

Figure 5. Excitation spectra of as-received (solid line), hydrated (dashed line), and hydrated plus VUV-irradiated PDP BAM (dotted line) for 450-nm emission from thick plaques, normalized at 305 nm. Note the feature at around 205 nm that is not present for other samples.

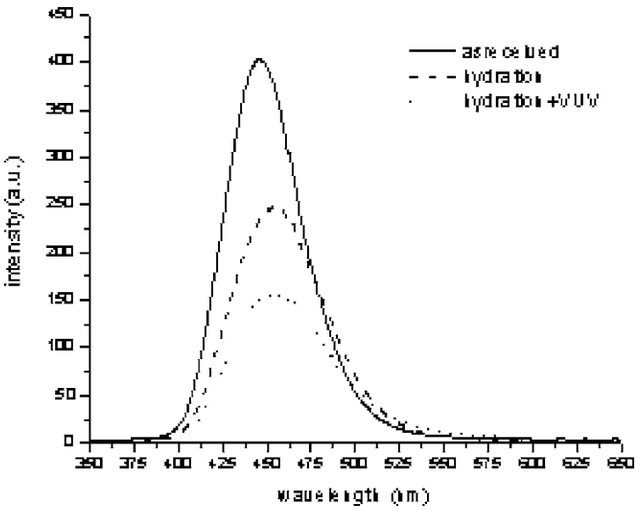

Figure 6. Emission spectra of as-received (solid line), hydrated (dashed line), and hydrated plus VUV-irradiated PDP BAM (dotted line) for 147-nm excitation.

The response of this PDP BAM to VUV excitation from a Xe discharge (147 nm) differs noticeably from the response to the UV excitation. As shown in Fig. 6, the emission spectra indicate a significant reduction in emission intensity for both the water-treated and VUV-irradiated samples. Relative to the fresh powder, the approximate change in total integrated radiance is about −25% for the thick hydrated sample and −50% after additional VUV irradiation. When the fresh sample is directly subjected to intense VUV radiation in VURAAC, the integrated emission drops by one third compared to the original. Thus, the degradation due to hydration and VUV irradiation appear to be additive and nearly independent of each other. Additionally, the higher intensity observed in the long-wavelength tail of both the hydrated and irradiated samples is not an artifact of normalization. The changes in emission spectra under 147- and 250-nm excitations are presented in Table VI.

We now analyze the structure of the 450-nm emission band. Its shape is asymmetrical, even on the energy scale[13,14] (Fig. 7). It is possible to explain this asymmetry by more than one factor: contributions from multiple luminescence centers, relatively weakly coupled electron-vibrational transitions (Huang-Rhys theory), and modification of the emission profile due to reabsorption of its high-energy wing. It is interesting to note that Eu^{2+} exhibits asymmetric band shapes in compounds with good cationic size match and one crystallographic, substitutional site, as in strontium fluoride and chloride[15] or oxide.[16]

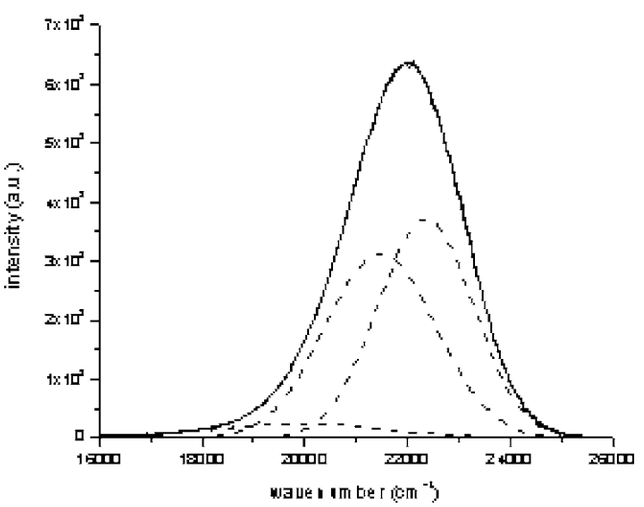

Figure 7. Fitting of the emission profile of as-received PDP BAM with three Gaussian functions.

A detailed and reliable analysis of this emission to unravel the asymmetry of the line shape is a far too complex and an assumption-laden task for any nonlinear data fitting procedure.[4,17,18] Results from Mössbauer spectroscopy indicate more than one type of Eu^{2+} ions to be present in the material. This leads to a question of how many of these centers actually participate in luminescence. It has been pointed out earlier[4] that the blue emission is very likely inhomogeneously broadened due to a distribution of emitting ions in distinct sites or with weakly varying bond parameters within the BAM structure. Emissions from multiple crystallographic sites, if present, are expected to be centered at various energies due to varying interaction strength between the europium 5d electron and the surrounding ions, notably oxygen. In addition, these emission components are likely broadened by random small-scale variations in their environment, as evidenced by large linewidths required for analysis of the observed Mössbauer line shapes in the investigated samples. Multiple emission components give rise to irregular line shapes in materials with more than one activator site.[19,20] In the analysis below, we have approximated the inhomogeneously broadened 450-nm emission envelope by a superposition of Gaussian functions, each of which represents a weakly inhomogeneous line shape associated with one site. This approximation is reasonable due to description of random strains that cause inhomogeneous broadening by normal distribution. It is also substantiated in light of a single configurational coordinate model in the harmonic approximation as well as theory of strongly coupled electron-vibrational transitions (with a large Huang-Rhys parameter S) that produce Gaussian-like profiles.[21,22] A weak to medium electron-phonon coupling predicts an asymmetric emission profile of a single luminescence center (e.g., band emission in $Al_2O_3:Cr^{3+}$).[21] We can argue, however, that the width of Eu^{2+} emission around 2500–3000 cm^{-1}, the lack of a zero-phonon line at cryogenic temperatures as measured for both crystals and powders,[d] and a considerable Stokes shift (estimated to be 4000 cm^{-1} at minimum) suggest strong electron-phonon coupling (including local vibrations). Last but not least, it is often argued that asymmetric line shapes arise from reabsorption of a portion of the high-energy side of emission, making the wing of the band fall off faster than a single Gaussian would permit.[14] We have investigated powders and single crystals with low Eu concentration and conclude that asymmetry persists despite considerable reduction in the density of absorbing centers. In addition, we investigated this possibility by accounting for potentially reabsorbed light in our fitting procedure and found little or no desired effect (see below).

We used area-normalized Gaussians to fit the emission profile of PDP BAM. The results for up to four components are presented in Table VII for as-received, hydrated, and hydrated-irradiated samples. The center wavelength, width, and change in size (compared to the one of as-received sample) are listed. As expected, the figure-of-merit (χ^2) improves with the number of components growing but it quickly becomes evident that most of the profile (besides the long wavelength tail) can well be approximated by two Gaussians only, typically located at around 450 and 470 nm. Additional components provide a better fit for the low-intensity tail region, bring nonconverging situations, or become nearly redundant from a luminescence point of view because of their area (small) and/or width (very large). Modification of emission profile by the reabsorption was investigated by measuring the reflectance of a thick plaque of the material (R_∞) and deriving the absorptance by $A_\infty = 1 - R_\infty$. The low-energy portion of this curve was approximated by three Gaussians to simulate the reabsorbed BAM emission. The peak en-

[d]Results will be presented in a separate paper.

Table VI. Spectral shifts of positions and widths of emission bands with corresponding changes for three PDP BAM samples investigated. Large variation in peak positions between 147- and 250-nm excitation is partly due to different calibration of the equipment.

	Excitation at 147 nm		Excitation at 250 nm	
Sample	Position/change (nm)	Width/change (cm^{-1})	Position/change (nm)	Width/change (cm^{-1})
As-received	445	2510	452	2520
Hydration	454/9	3000/490	460/8	2850/330
Hydration + VUV	456/11	3060/550	460/8	2890/370

ergies of these three components closely coincide with the ones found in our earlier work.[12] These positions and widths of the three Gaussians having negative areas were at first used as fixed parameters in the emission curve-fitting procedure. The areas of the Gaussians were allowed to change with their mutual ratios locked, as determined from the absorption fit and mirroring proportionality to the light absorbed by plaque in the reflectance measurement. Despite accounting for reabsorbed photons this way, at least two components besides the "loss" Gaussians were needed to describe the line shape and the fit at high-energy side was not good.

It is evident from Table VII that nearly independent of the number of Gaussian components used for fitting ($n \geq 2$), the ones located on the shorter wavelength side of the peak lose and the ones at longer wavelengths gain their area due to the degradation process. However, the present fitting procedure is not reliable for deciding how many components actually exist or are needed to fully describe the emission curve. It is unlikely, though, that more than three major components are actually required. Figure 7 presents the fitting results for this case.

Discussion

We have presented in the previous sections a number of observations regarding the maintenance of BAM following the water treatment. At first sight, some of the experimental results appear to be contradictory. In order to develop methods to control the degradation process induced by intercalation of water into the BAM lattice, the mechanisms of oxidation of activator ions and green shift of the emission band of the hydrated BAM phosphor samples should be clearly understood. We recall that the green shift of the emission band is also observed in phosphors aged in fluorescent lamps as well as in phosphor samples exposed to 185-nm radiation. Some of this degradation can be recovered upon heating in air at moderate temperatures. Heating as-prepared BAM above 400°C in air leads to oxidation of europium ions, which is accompanied by emission blue shift.[5] This oxidative degradation does not occur if the phosphor is heated in a neutral (nitrogen) atmosphere. This way, it is possible to recover most of the brightness in water-damaged samples. Interestingly, oxidative degradation shows significant spontaneous recovery over long time periods (1–2 years), whereas radiation-induced changes in emission appear to be relatively more permanent.

Despite the considerable shift and widening of the emission band of hydrated BAM, its total integrated area for infinitely thick plaques is reduced by only 4% for the 250-nm excitation. For excitation at 147 nm, the reduction of integrated intensity is close to 25%. The Mössbauer measurements suggest that the occupancy of site 1 (assigned to mO position) drops from 30 to 22%, whereas sites 2 and 3 (assigned to BR and aBR positions) are affected less. The total reduction in Eu^{2+} (from Tables I and II) is 12%. Yet, both the 250-nm excitation and γ-radiation in Mössbauer measurements supposedly interact with all the Eu ions in the material. This apparent discrepancy between Mössbauer and fluorescence measurements can be explained qualitatively by assuming not all the oxidized Eu^{2+} having participated in the luminescence process. Let us examine the fluorescence and reflectance measurements more closely. Figure 4 shows the reduction in absorption coefficient upon hydration being concentrated around 290–350 nm, whereas at 250 nm this parameter exhibits practically no change. The two major absorption bands have their peak values more or less equalized after heating in water vapor (with slightly lower values at 305 nm compared to 250 nm). Furthermore, there is additional absorption appearing at 255–285 nm, which does not contribute to the excitation spectrum (Fig. 5). Normalization of the excitation spectra shows that the excitation efficiency has been reduced at 250 nm relative to 305 nm. Together, these changes imply the loss of quantum efficiency of the material at 250 nm due to a smaller fraction of incident photons being absorbed by Eu^{2+} after hydration. The absorption band appearing at around 255–285 nm competes with the remaining Eu^{2+} ions at these wavelengths and beyond but evidently does not add to the blue emission. At the same time, the part of absorption removed in the 290–350 nm range has not adversely affected the excitation efficiency there. Scaling of the two excitation curves (viz. for as-received and hydrated

Table VII. Deconvolution of thick plaque emission profiles of as-received, water-treated, and VUV-irradiated samples of PDP BAM under 250-nm excitation using up to four Gaussians. Peak wavelength, fwhm, and corresponding area changes upon treatment for each Gaussian are indicated.

	As-received		Water-treated			VUV-irradiated		
Sample No. of G	λ (nm)	fwhm (cm^{-1})	λ (nm)	fwhm (cm^{-1})	Area change (%)	λ (nm)	fwhm (cm^{-1})	Area change (%)
1G	456	2647	462	2901	−3	456	2661	−11
2G	477	3039	480	3061	+30	480	3187	−17
	452	2371	457	2555	−15	453	2398	−8
3G	502	3902	489	3313	+181	510	4250	−11
	466	2535	464	2540	+39	467	2582	−15
	447	2186	442	2017	−69	448	2203	−5
4G	518	4511	497	3643	+150	522	4761	+12
	471	2703	469	2667	+72	471	2736	−9
	451	2269	450	2278	−50	451	2269	−12
	431	861	431	855	−35	431	897	0

samples) at 250 nm according to their 4% difference in total emission is essentially producing the equivalent of Fig. 5, with very little loss of excitation at 305 nm. In other words, a major part of the divalent europium ions that were oxidized did not participate in the emission process to start with. These data reflecting the wavelength-dependent reduction in absorption coefficient support the existence of multiple sites of europium in BAM. A decrease by one quarter in site 1 population of Eu^{2+} (Tables I and II) can be speculated to relate to about 20% change of absorption coefficient at 305 nm (Fig. 4).

Regarding the VUV excitation, we assume the absorption coefficient of the phosphor layer not to be significantly affected by hydration near 147 nm. The strong host absorption itself dominates the process and the photon penetration is limited to the surface layers of each particle. The intercalation process, being diffusion limited, possibly results in higher concentration of water molecules close to the surface and thus, in higher Eu^{3+} concentration there. This reduces the number of available Eu^{2+} ions for radiative recombination. Thus, the hydration process significantly affects the phosphor performance for excitations above the bandgap energy, as confirmed by our measurements. We note the relatively larger spectral changes upon hydration and VUV irradiation for 147-nm excitation compared 250 nm (Table VI). The loss of emission may be enhanced due to confinement of exciting radiation closer to the surface of particles rather than in the bulk that potentially causes saturation of excitation.[23]

We may speculate over the nature of the appearing absorption in the 255–285 nm range. Eu^{3+} charge-transfer (CT) transitions in oxide lattices typically occur in this region. Supported by the data on increasing trivalent europium concentration in Tables I and II, we assign this absorption to ligand-activator CT mechanism. The lack of emission from trivalent ions despite the confirmation of their abundance via Mössbauer spectroscopy in both as-received and hydrated samples is puzzling. The luminescence could be missing due to total quenching of emission or energy transfer. The characteristic trivalent europium emission from the $^5D_0 \rightarrow {}^7F_2$ transition at a site without inversion symmetry is known to be hypersensitive, whose efficiency depends critically on the environment. The possibility is that the local environment of the Eu^{3+} ions generated during the oxidation process is not favorable for efficient fluorescence. Another possibility involving energy transfer from Eu^{3+} to some other center requires more detailed experiments that are beyond the scope of this paper.

Increased excitation efficiency around 205 nm could be attributed to the formation of color centers (F-centers) that, after absorbing a part of energy, readily transfer to Eu^{2+}. Alternatively, one can assume rearrangement of europium ions in the lattice that brings along a change in environment and therefore a noticeably altered excitation spectrum for a small part of Eu^{2+}.

We analyze two plausible models that could explain at the microscopic level the observed green shift of the emission spectrum and oxidation of europium ions. The first model is based on the assumption that the two observations characterizing degradation of BAM are independent of each other. The intercalated water molecules or hydroxyl groups could have caused the green shift, and oxygen in the humid air could have been responsible for the oxidation of the europium ions. Because intercalation of water is a reversible process, on desorbing the water molecules the original spectral profile could be restored. Thus, the water-induced degradation is a combined effect of normal oxidative degradation, and the spectral shift caused by adjacent water molecules or hydroxy radical. This picture implies that the green shift induced by water is distinct from the VUV-induced degradation. There should also be no recovery of oxidation state of activator ions on desorbing water molecules.

The other model is based on the assumption that both oxidation of europium ions and green shift of the emission spectrum are caused by the intercalation process. Oxygen partial pressure in the humid air is not driving the oxidation process. The green shift in the emission is caused by the presence of water molecules or hydroxyl groups in the lattice as result of the intercalation process.

The oxidation of europium ions begins with the water molecules dissociating to hydroxyl groups

$$(Ba_{Ba})^X + (H_2O)^X \rightleftharpoons (Ba_{Ba} - -OH^-)' + (H_I^+)^{\cdot} \quad [1]$$

The proton released from this solid-state interaction could form hydronium ions with other water molecules or generate hydroxyl group with other oxygen atoms in this oxygen-rich lattice. These protons could also lead to oxidation of the divalent Eu ions

$$(H_I^+)^O + (Eu_{Ba}^{2+})^X \rightleftharpoons (Eu_{Ba}^{3+})^{\cdot} + \tfrac{1}{2}H_2\uparrow \quad [2]$$

Chemical reactions 1 and 2 imply release of hydrogen molecules during the oxidation of europium ions. This oxidation process could occur in neutral but humid atmosphere and would not require oxygen. The oxidized europium ions can be partially reduced back to its divalent state by the hydroxyl groups generated during the intercalation process

$$2(Eu_{Ba}^{3+})' + 2(Ba_{Ba}^{2+} - -OH^-)^{\cdot} \rightleftharpoons 2(Ba_{Ba}^{2+})^X + 2(Eu_{Ba}^{2+})^X + \tfrac{1}{2}O_2\uparrow + \tfrac{1}{2}H_2O\uparrow \quad [3]$$

Conclusion

The main objective of the present study was to determine if intercalation of water leads to oxidation of activator ions and to understand the modifications in the emission spectrum of the BAM phosphor. A comparison of ^{151}Eu Mössbauer spectra of BAM samples before and after intercalation of water molecules clearly reveals the increase in trivalent europium concentration. Optical spectroscopy measurements analyzed in this work confirm the green shift of the emission spectrum and shed some light on the coexistence of Eu^{2+}/Eu^{3+} ions in both as-received and hydrated BAM. As expected, the predominant negative effect of hydration occurs on the blue side of the Eu^{2+} emission band, whereas the long wavelength contribution increases. We assign the cause for both oxidation of europium and emission green shift to the intercalation of water into BAM. Absorption due to Eu^{3+} formed during the hydration process practically compensates for the reduced absorption of Eu^{2+} ions in the short-wavelength region but not around the 305-nm band. No significant emission from the trivalent europium ions in hydrated samples was observed down to liquid helium temperatures. It is plausible that quenching of Eu^{3+} emission takes place due to its immediate environment or is mediated by energy transfer to other centers.

Orsam Sylvania assisted in meeting the publication costs of this article.

References

1. S. Oshio, T. Matsuoka, S. Tanaka, and H. Kobayashi, *J. Electrochem. Soc.*, **145**, 3903 (1998).
2. S. Oshio, K. Kitamura, T. Nishiura, T. Shigata, S. Horii, and T. Masuoka, *National Tech. Report*, 43, 181 (1997).
3. K. Yokota, S. Zhang, K. Kimura, and A. Sakamoto, *J. Lumin.*, **92**, 223 (2001).
4. A. Ellens, F. Zwaschka, F. Kummer, A. Meijerink, M. Raukas, and K. C. Mishra, *J. Lumin.*, **93**, 147 (2001).
5. P. Boolchand, K. C. Mishra, M. Raukas, A. Ellens, and P. C. Schmidt, *Phys. Rev. B*, **66**, 134429 (2002), and references therein.
6. T. H. Kwon, M. S. Kang, J. P. Kim, and G. J. Kim, *J. Soc. Inf. Disp.*, **10**, 241 (2002).
7. T. Onimaru, S. Fukuta, T. Misawa, K. Sakita, and K. Betsui, *SID Symposium*, May 2004.
8. J. B. Bates, N. J. Dudney, G. M. Brown, J. C. Wang, and R. French, *J. Chem. Phys.*, **77**, 4838 (1982).
9. N. J. Dudney, J. B. Bates, and J. C. Wang, *J. Chem. Phys.*, **77**, 4857 (1982).
10. K. C. Mishra, In preparation (2005).
11. M. Stephan, P. C. Schmidt, K. C. Mishra, M. Raukas, A. Ellens, and P. Boolchand, *Z. Phys. Chem. (Munich)*, **215**, 1397 (2001).
12. K. C. Mishra, M. Raukas, A. Ellens, and K. H. Johnson, *J. Lumin.*, **96**, 95 (2002).
13. K. H. Butler, *Fluorescent Lamp Phosphors*, Chap. 12, The Pennsylvania State University Press, University Park, PA (1980).
14. G. Blasse and B. C. Grabmaier, *Luminescent Materials*, Springer-Verlag, Berlin (1994).
15. T. Kobayasi, S. Mroczkowski, J. F. Owen, and L. H. Brixner, *J. Lumin.*, **21**, 247 (1980).
16. N. Yamashita, *J. Lumin.*, **59**, 195 (1994).

17. W. H. Press, B. P. Flannery, S. A. Teukolsky, and W. T. Vetterling, *Numerical Recipes*, Cambridge University Press, Cambridge (1986).
18. G. K. Wertheim, M. A. Butler, K. W. West, and D. N. E. Buchanan, *Rev. Sci. Instrum.*, **45**, 1369 (1974).
19. A. Diaz and D. A. Keszler, *Chem. Mater.*, **9**, 2071 (1997).
20. K. Machida, G. Adachi, and J. Shiokawa, *J. Lumin.*, **21**, 101 (1979); S. H. M. Poort, W. P. Blokpoel, and G. Blasse, *Chem. Mater.*, **7**, 1547 (1995).
21. B. Henderson and G. F. Imbusch, *Optical Spectroscopy of Inorganic Solids*, Chap. 5, Clarendon Press, Oxford (1989).
22. D. Curie, in *Optical Properties of Solids*, B. Di Bartolo, Editor, pp. 71–106, Plenum Press, New York (1975).
23. K. C. Mishra and M. Raukas, *J. Electrochem. Soc.*, **151**, H105 (2004).